DESIGN OF A BISTABLE ROBOT LEG USING LEAF-OUT ARCHITECTURE

Chaewon Baek

cwb1207@snu.ac.kr

Department of Mechanical Engineering, Seoul National University

ABSTRACT

In this project, a bistable origami leg with a unique property is designed: The structure is modeled using Fusion 360 and is prototyped through 3D printing.
Since the leaf-out architecture is rigid foldable, the structure is analyzed through loop closure method, and simulated with paraview. The stability of the model is analyzed by torsional spring method [2-3]. The trajectory of the endpoint of the appendage is obtained through loop closure method. The energy curves of the model shows that the designed appendage is bistable.
Also, the various variations of the end curve of the leg shows parameters of the structure might be optimized through methods such as machine learning so that the total trajectory of the endpoint of the structure follows that of a traditional robot leg.

1. INTRODUCTION

Origami waterbomb base is one of the most elementary structures in the history of origami [2]. The most interesting aspect of the said model is that it exhibits bistability, similar to the bistable snap-through mechanism [1]. Leaf-out architecture can be considered as a variation of the traditional waterbomb base, and the kinematics of the structure has been extensively investigated [3]. Using the structure, a gripper that is triggered by external force has been demonstrated [4].

In this project, a bistable origami leg with a unique property is demonstrated: First, I design and fabricate a prototype of the model using 3d printing. I then use a rigid origami model to characterize the unique kinematics of the structure and analyze the energy barrier and the trajectory of the endpoint of the structure.

2. MATERIALS AND METHODS

2.1 Fabrication of the prototype

Before analyzing the properties of the structure through rigid origami simulation, a prototype is fabricated through 3D printing. Each crease line is modeled as hinge structure using Hoberman technique [5]. Fusion360 is used for modeling and initial verification of the model's kinematic behavior. FDM Filament and 3D printer Ultimaker 2+ Connect is utilized for printing. Since 3D printing is a method that laminates melted plastic layer by layer, interference between parts may arise from thermal distortion and limited resolution of the nozzle. To avoid this, the prototype is designed to have 0.2mm gap between parts. Along with the printed parts, brass wire of thickness 0.2mm is used to serve as a rotational axis between the parts. Interestingly, the finished model showed self-locking behavior in the fully folded configuration: Although forces exerted to the endpoint of the structure is expected to unfold the model, the model showed resistivity to the force applied at lengthwise direction of the last part of the leg. Figure 1, 2 shows the cad model of the structure. Figure 3, 4, 5 shows the assembled model.

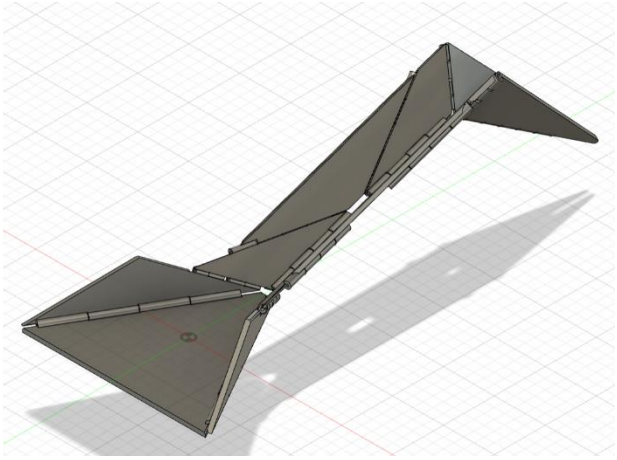

Figure 1: Unfolded configuration of cad model

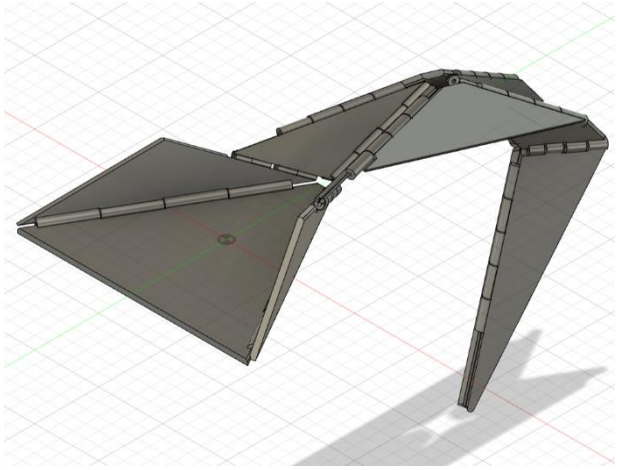

Figure 2: Folded configuration of cad model

Figure 3: Unfolded configuration of the prototype

Figure 4: Folded configuration of the prototype

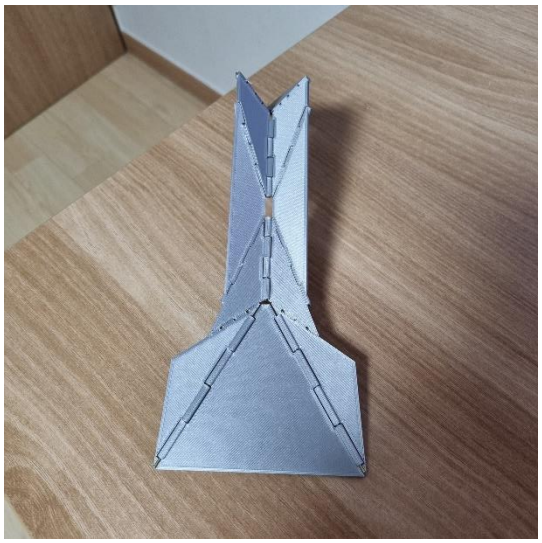

Figure 5: Flat configuration of the prototype

2.2 Leaf-out bistable leg model

Figure 6 shows the fundamental geometry and the input parameters used to initialize the model. Figure 7 shows the notation for the vertices and fold angle for the edges of the model.

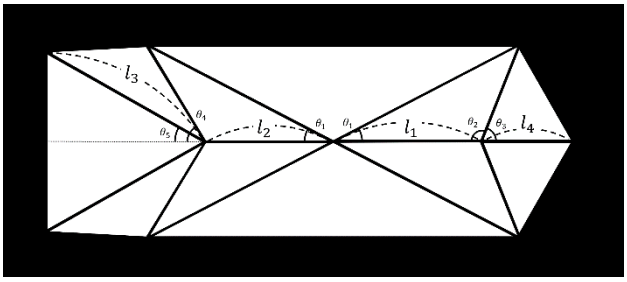

Figure 6: Parameters of the simulation model

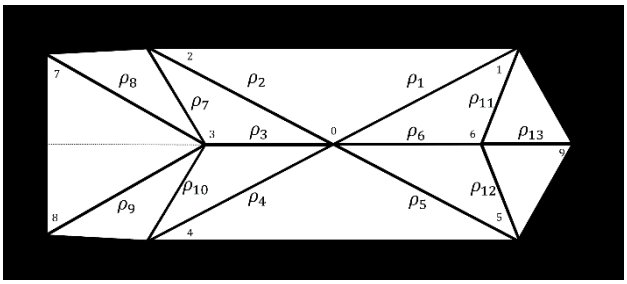

Figure 7: Notation for the vertices and fold angles

Figure 8: Theta 3

It must be taken into account that although θ_3 shown in Figure 6 seems planar, it is not. Figure 8 depicts acutely of the situation. Also, to constrain the model such that it moves in mirror image with respect to the middle line, following constraints were imposed upon the model:

$$\rho_1 = \rho_5$$
$$\rho_2 = \rho_4$$
$$\rho_7 = \rho_{10}$$
$$\rho_8 = \rho_9$$
$$\rho_{11} = \rho_{12}$$

To simulate the model, we introduce rigid origami simulation technique [6]. First, the loop closure constraint around vertices is considered. For each vertices, a linearized constraint matrix is obtained through rotation matrix operations and derivatives of the loop closure constraint matrix. Summing up each constraint matrix C, a global linearized constraint matrix is formed from which the iterations the increment folding angle from the iterations of each folding step can be calculated through additional usage of Moore/Penrose pseudoinverse matrix of C. Also, to account for the accumulation of numerical error, residual components are calculated from the loop

closure constraint matrix and calculated increment folding angle. Using the errors obtained, the answer is corrected. The above method is carried out using custom made python code to generate the model. The model is then processed as a vtk file format and visualized through the simulation program Paraview. Based on the rigid origami simulation, an energy analysis by modeling crease lines as a linear torsion spring is carried out.

However, using pure rigid origami simulation for the whole model failed due to unknown reasons. Since the residual matrix showed drastic increase around vertex 6, I speculate that the model failed due to the initially non-planar state that resembles saddle-like geometry, though the simulation technique must work for all rigid origami models.

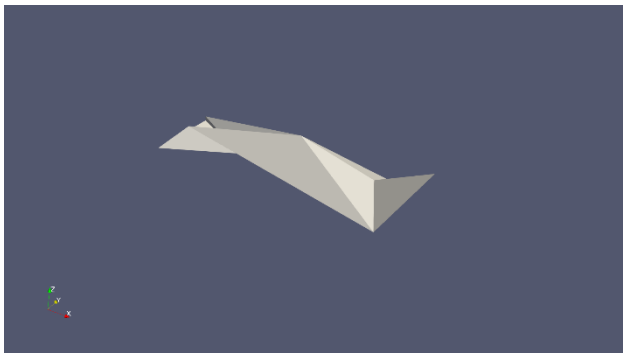

Figure 9: The failed model

A second method was devised in order to obtain the correct angles for the whole model: although all angles excluding the $\rho_{11}, \rho_{12}, \rho_{13}$ were obtained through rigid origami simulation as before, $\rho_{11}, \rho_{12}, \rho_{13}$ were calculated analytically from the numerically obtained ρ_6 and cross product and dot product of the vectors. The process is as follows, using the notations from Figure 10.

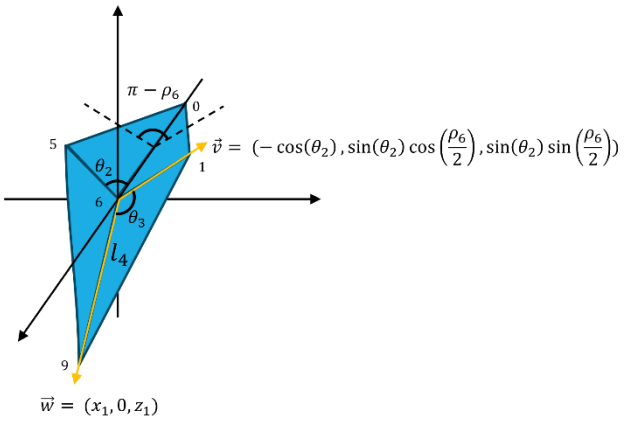

Figure 10: Analytical approach

$$x_1^2 + z_1^2 = 1$$
$$\overrightarrow{w} \cdot \vec{v} = \cos(\theta_3)$$
$$\vec{w} \times \vec{v} = (n_1, n_2, n_3)$$

$$\frac{(\vec{w} \times \vec{v}) \cdot (\vec{v} \times (-1, 0, 0))}{\sin(\theta_2)\sin(\theta_3)} = \cos(\rho_{11})$$

$$\frac{(n_1, n_2, n_3) \cdot (n_1, -n_2, n_3)}{|n|^2} = \cos(\rho_{13})$$

Using the five equations above, $\rho_{11}, \rho_{12}, \rho_{13}$ can be calculated for any configuration of the model. Applying the new method, a robust model that showed no unexpected movements deviating from the expected path was generated and is shown in Figure 11, Figure 12.

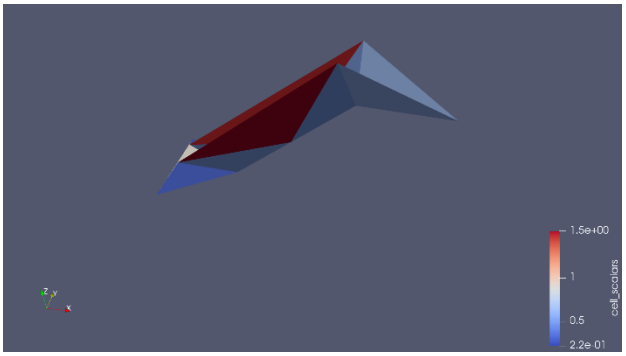

Figure 11: Unfolded configuration of the model

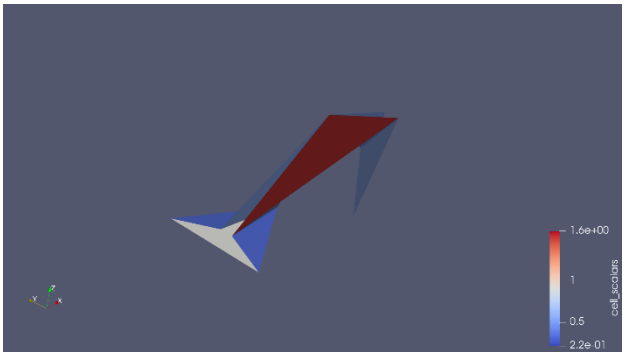

Figure 12: Folded configuration of the model

2.3 Results

In this section, we obtain various potential energy curves by varying the input parameters. Figure 13 to 16 shows the energy landscape for various configurations.
l_1, l_2, l_3, l_4 are all equally input as 1.
For all models, the energy graph showed clear difference between the folded configuration and unfolded configuration. Starting from the lowest energy configuration, which is the fully folded configuration, the energy gradually gets higher as ρ_3 is unfolded. The maximum peak is at $\rho_3 = 0°$, which corresponds to the flat configuration. From the flat configuration, the model transition into either the unfolded configuration, or the folded configuration, hence bistability is shown.

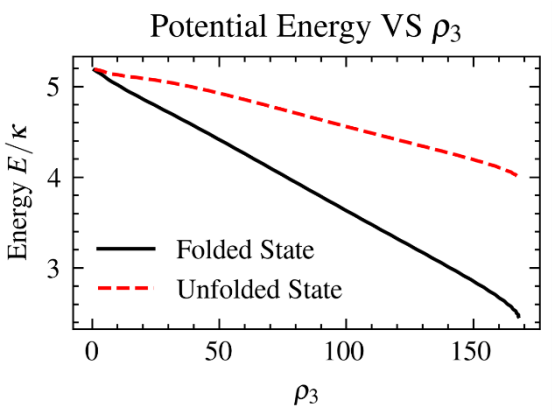

$\theta_1 = 22.5°, \theta_2 = 100°, \theta_3 = 100°, \theta_4 = 55°, \theta_5 = 30°$

Figure 13

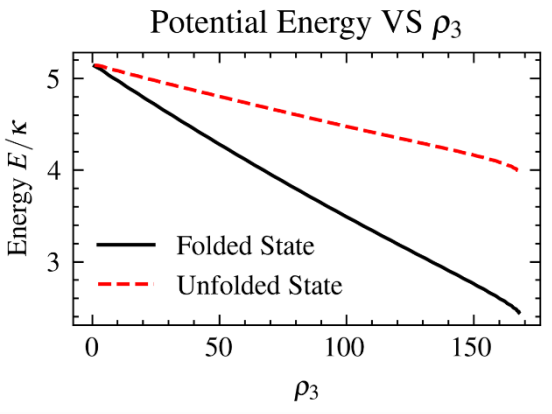

$\theta_1 = 22.5°, \theta_2 = 120°, \theta_3 = 100°, \theta_4 = 55°, \theta_5 = 30°$

Figure 14

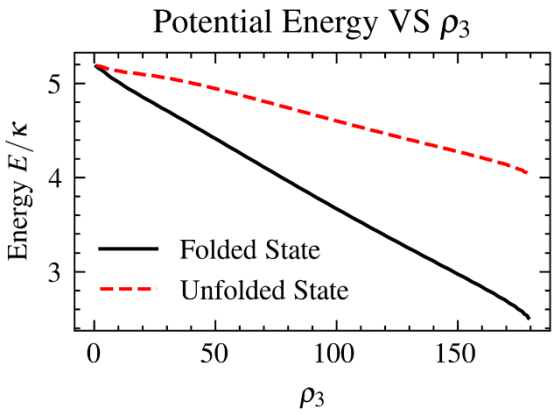

$\theta_1 = 30°, \theta_2 = 100°, \theta_3 = 100°, \theta_4 = 60°, \theta_5 = 30°$

Figure 15

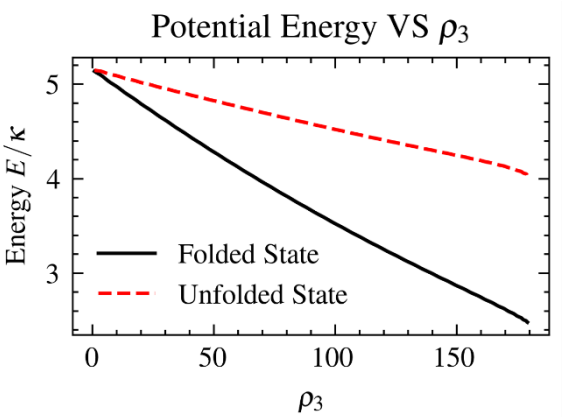

$\theta_1 = 30°, \theta_2 = 120°, \theta_3 = 100°, \theta_4 = 60°, \theta_5 = 30°$

Figure 16

It seems worth noting that the overall shape of the graph remains the same for all configurations, although this may be since the variations between the parameters were small. Varying the parameters more than $20°$ had unexpected errors emanating from the built-in methods of the python code, which limited the scope of the analysis.

Also, the trajectory of the endpoint of the structure was graphed from Figure 17 to Figure 20. In contrast to the potential energy graphs, the trajectory graph showed clear differences even for small variations of the parameters.

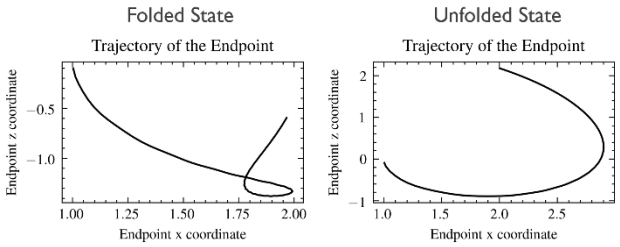

$\theta_1 = 22.5°, \theta_2 = 100°, \theta_3 = 100°, \theta_4 = 55°, \theta_5 = 30°$

Figure 17

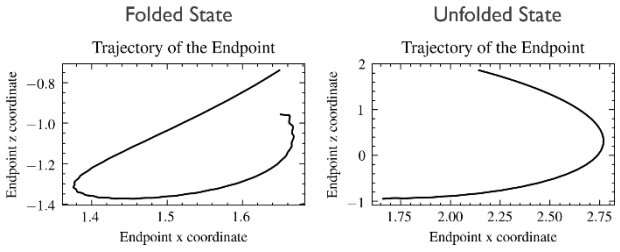

$\theta_1 = 22.5°, \theta_2 = 120°, \theta_3 = 100°, \theta_4 = 55°, \theta_5 = 30°$

Figure 18

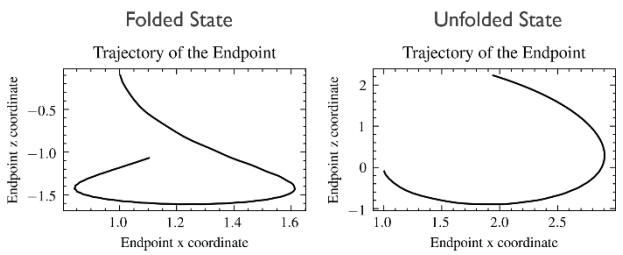

$\theta_1 = 30°, \theta_2 = 100°, \theta_3 = 100°, \theta_4 = 60°, \theta_5 = 30°$

Figure 19

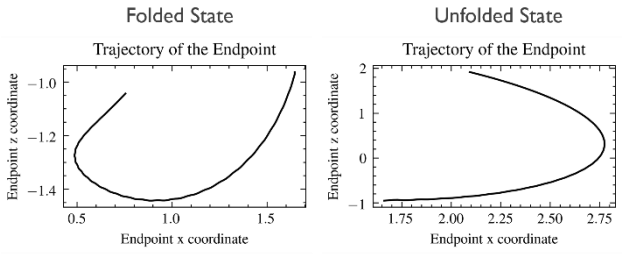

$\theta_1 = 30°, \theta_2 = 120°, \theta_3 = 100°, \theta_4 = 60°, \theta_5 = 30°$

Figure 20

CONCLUSION

I have designed and prototyped a bistable origami leg with a unique property, and numerically studied the behavior of the architecture. I found out that the imposed model exhibits a bistable energy landscape, although it is uncertain if the shape of the graph is tailorable due to limited analysis method.

Also, the prototype showed self-locking properties: it seems that the designed appendage is stable and can withstand external load at certain direction in folded state without needing forces other than those emanating from its structural uniqueness.

Lastly, I found that the end point of the leg moves very sensitive to the input parameters. The parameters of the structure may be adjusted to make linkages for special purposes, such as appendages for walking or drill arms for rock sampling in space. Various optimization algorithms such as gradient descent or machine learning might be applied to find the needed input values.

REFERENCES

[1] Hussein, H., Younis, M. I., 2020, “Analytical Study of the Snap-Through and Bistability of Beams with Arbitrarily Initial Shape”, J. Mech. Robot., 12(4), p. 041001.

[2] Hanna, B. H., Lund, J. M., Lang, R. J., Magleby, S. P., and Howell, L. L., 2014, “Waterbomb Base: A Symmetric Single-Vertex Bistable Origami Mechanism”, Smart Mater. Struct., 23(9), p. 094009.

[3] Yasuda, H., Chen, Z., Yang, J., 2016, “Multitransformable Leaf-Out Origami with Bistable Behavior”, J. Mech. Robot., 8(3), p. 031013.

[4] Yasuda, H., Johnson, K., Arroyos, V., Yamaguchi, K., Raney, J. R., Yang, J., 2022, “Leaf-like Origami with Bistability for Self-Adaptive Grasping Motions”, Soft Robot., 9(5), p. 938-947.

[5] Lang, R. J., Nelson, T., Magleby, S. P., and Howell, L. L., 2017, “Thick Rigidly Foldable Origami Mechanisms Based on Synchronized Offset Rolling Contact Elements”, J. Mech. Robot., 9(2), p. 021013.

[6] Tachi T, Peters AK. Simulation of Rigid Origami. Natick, MA: R. J. Lang, 2009.